Published in Journal of the Optical Society of America A 20, issue 10, 1969-1973, 2003
which should be used for any reference to this work

Application of the boundary-element method to the interaction of light with single and coupled metallic nanoparticles

Carsten Rockstuhl, Martin Guy Salt, and Hans Peter Herzig

University of Neuchâtel, Institute of Microtechnology, Rue A.-L. Breguet 2, CH-2000 Neuchâtel, Switzerland

The boundary-element method is applied to the interaction of light with resonant metallic nanoparticles. At a certain wavelength, excitation of a surface plasmon takes place, which leads to a resonantly enhanced near-field amplitude and a large scattering cross section. The resonance wavelength for different scatterer geometries is determined. Alteration of the scattering properties in the presence of other metallic nanoparticles is discussed. To treat this problem, a novel formulation of the boundary-element method is presented that solves the interaction problem for all the coupled particles.

1. INTRODUCTION

When metallic nanoparticles are illuminated at an appropriate wavelength, excitation of surface plasmons can take place. Surface plasmons are a collective oscillation of free electrons within the material.[1] The excitation leads to a resonantly enhanced near-field amplitude and a large scattering cross section (SCS) for a narrow wavelength band. The principal effect has been known for centuries. Unfortunately, the conditions for the appearance of the resonances can be predicted only analytically in the case of elliptical particles within the electrostatic limit (dimensions much smaller than the wavelength).[2] For example, in the ideal case of an infinite circular cylinder surrounded by air,[3] the material must have a relative complex permittivity of $\epsilon_{2D} = -1$ and a sphere of $\epsilon_{3D} = -2$. Silver and gold are two materials that approximately fulfill this condition. Their resonances appear in the blue region of the visible spectrum. For other structures and even for the exact solution of spherical particles that have a finite feature size, prediction of the scattering properties requires an exact solution of Maxwell's equations. Over time, various numerical tools have been applied to the problem: Moreno *et al.* used the multiple multipole method (MMM),[4] Yang *et al.* used the discrete dipole approximation (DDA),[5] and Kottmann and Martin in a series of pioneering publications applied Green's dyadic function.[6,7]

In the present work we have used the boundary-element method (BEM) to simulate the interaction of light with resonant metallic nanoparticles. An advantage of this method is its numerical stability and the relatively easy incorporation of additional scatterers and subsequent solution of the coupled-particle problem.

2. SCATTERING CROSS SECTION AND NEAR-FIELD AMPLITUDES FOR A SINGLE PARTICLE

The BEM is a well-known technique in fields such as acoustics, fluid mechanics, elasticity, and fracture mechanics.[8] But only a few authors have applied this method to microoptical problems. The method has been used mainly for analyzing the diffraction properties of mirrors,[9] layered spheres,[10] and cylindrical microlenses.[11] The present implementation is based on some pioneering work conducted by Prather *et al.*,[12,13] who applied the method to Fresnel lenses.

The basic two-dimensional scattering problem consists of a homogeneous scatterer with a relative permittivity of ϵ_I. The scatterer is described by its surface contour C and its outward normal $\hat{n}_I$. The structure is invariant in the third dimension z and is illuminated by an incident wave field $u^{\mathrm{inc}}(\rho)$ from a region with a homogeneous permittivity ϵ_0. ρ is an observation point in the $x-y$ plane. If the incoming field is TE polarized, the field component $u(\rho)$ denotes the $E_z(\rho)$ component of the electric field. If the field is TM polarized, $u(\rho)$ denotes the magnetic field component $H_z(\rho)$. For both cases the total field $u^{\mathrm{tot}}(\rho)$ is the sum of the incoming field $u^{\mathrm{inc}}(\rho)$ and the scattered field $u^{\mathrm{sc}}(\rho)$. The normal derivatives of the different fields with respect to the boundary are denoted by $v^{\mathrm{inc}}(\rho)$, $v^{\mathrm{sv}}(\rho)$, and $v^{\mathrm{tot}}(\rho)$, respectively. It is assumed that the materials are nonmagnetic, i.e., that the relative permeability is $\mu_r = 1$.

The total field in the interior region has to be a solution of the homogeneous wave equation, and in the exterior region it has to be a solution of the inhomogeneous wave equation, because of the presence of an additional source

term $f(\rho)$. The source term describes in principle the incident wave field. The wave equations are

$$\begin{aligned} 0 &= \nabla^2 u_I^{\mathrm{tot}}(\rho) + k_I^2 u_I^{\mathrm{tot}}(\rho) \quad \text{for } \rho \in I, \\ -f(\rho) &= \nabla^2 u_O^{\mathrm{tot}}(\rho) + k_O^2 u_O^{\mathrm{tot}}(\rho) \quad \text{for } \rho \in O, \end{aligned} \tag{1}$$

with $k_{I,O} = (2\pi\sqrt{\epsilon_{I,O}})/\lambda_0$ being the wave number in the interior (I) and the exterior (O) region, respectively. Applying Green's second identity, we can derive the boundary integral equations[12]:

$$\begin{aligned} 0 = u^{\mathrm{sc}}(\rho) &+ \int_C \left\{ u^{\mathrm{sc}}(\rho') \frac{\partial G_I(\rho,\,\rho')}{\partial \hat{n}_I} \right. \\ &\left. - p_I G_I(\rho,\,\rho') v^{\mathrm{sc}}(\rho') \right\} \mathrm{d}l' \\ &+ u^{\mathrm{inc}}(\rho) + \int_C \left\{ u^{\mathrm{inc}}(\rho') \frac{\partial G_I(\rho,\,\rho')}{\partial \hat{n}_I} \right. \\ &\left. - p_I G_I(\rho,\,\rho') v^{\mathrm{inc}}(\rho') \right\} \mathrm{d}l' \quad \text{for } \rho \in I, \end{aligned}$$

$$\begin{aligned} 0 = u^{\mathrm{sc}}(\rho) &+ \int_C \left\{ p_O G_O(\rho,\,\rho') v^{\mathrm{sc}}(\rho') \right. \\ &\left. + u^{\mathrm{sc}}(\rho') \frac{\partial G_O(\rho,\,\rho')}{\partial \hat{n}_O} \right\} \mathrm{d}l' \quad \text{for } \rho \in O, \end{aligned} \tag{2}$$

where $u^{\mathrm{inc}}(\rho)$ and $u^{\mathrm{sc}}(\rho)$ are the field values along the contour and the remaining integral terms describe the scattered contribution of the scattered field from each point of the surface. It should be kept in mind that the contour normal pointing in the exterior space has a sign different from that pointing in the interior space; i.e., $\hat{n}_I = -\hat{n}_O$. $G_{I,O}$ are the two-dimensional free-space Green's functions in the interior and exterior regions, and $p_{I,O}$ is a factor that depends on the polarization: $p_{I,O} = 1$ for TE polarization and $p_{I,O} = \epsilon_{I,O}$ for TM polarization. Equation (2) can be cast into a set of linear equations by expanding the unknown scattered field $u^{\mathrm{sc}}(\rho)$ and its normal derivative $v^{\mathrm{sc}}(\rho)$ in terms of linear interpolation functions across the surface.[12] Solution of this system of linear equations gives the unknown scattered field and its derivative at the nodal points. The scattered field can then be calculated everywhere in space by using

$$\begin{aligned} u^{\mathrm{sc}}(\rho) = \int_C \Bigg[& u^{\mathrm{sc}}(\rho') \frac{\partial G_O(\rho,\rho')}{\partial \hat{n}_I} \\ & - p_O G_O(\rho,\,\rho') v^{\mathrm{sc}}(\rho') \Bigg] \mathrm{d}l'. \end{aligned} \tag{3}$$

In a final step, the total field is calculated by adding the field distribution of the incoming wave. A detailed derivation can be found in Refs. 12 and 13.

The aim of this work is to describe systems that consist of more than a single scatterer. To incorporate additional scatterers in the formulation, the incoming wave field $u_m^{\mathrm{inc}}(\rho)$ on particle m is written as

$$\begin{aligned} u_m^{\mathrm{inc}}(\rho_m) = u_0^{\mathrm{inc}}(\rho_m) + \sum_{n \neq m} \int_C \Bigg[& u_n^{\mathrm{sc}}(\rho_n') \frac{\partial G_O(\rho_m\,,\,\rho_n')}{\partial \hat{n}_I} \\ & - p_O G_O(\rho_m\,,\,\rho_n') v_n^{\mathrm{sc}}(\rho_n') \Bigg] \mathrm{d}l', \end{aligned} \tag{4}$$

where $u_0^{\mathrm{inc}}(\rho_m)$ is the illuminating-source wave field on particle m and the second term describes the contribution of the scattered wave field from each other particle n on particle m. A similar expression can be found for the field derivatives of the new incoming wave field $v_m^{\mathrm{inc}}(\rho_m)$. Inserting Eq. (4) into Eq. (2) makes it possible to derive a system of linear equations similar to that in the classical BEM, but now the equation solves the coupled interaction for all particles. Once this system is solved, the scattered field and its derivative along the surface of each scatterer is known. The entire field is finally just a superposition of the incoming wave field and the contribution from each scatterer, calculated by Eq. (3).

In the present work we have concentrated on silver as the particle material. Its negligible imaginary part of the permittivity function in the region of interest promises sharp and strong resonant behavior over a small wavelength band. First, simulations were made partly by using a Drude model. The dielectric constant is given by[4]

$$\epsilon_{\mathrm{Ag}}(\nu) = 1 + \frac{i\tau\omega_p^2}{2\pi\nu(1 - i2\pi\tau\nu)}, \tag{5}$$

with the relaxation time $\tau = 1.45 \times 10^{-14}\,\mathrm{s}$ and the plasma frequency $\omega_P = 1.32 \times 10^{16}\,\mathrm{rad\,s^{-1}}$.

Excitation of plasmons is possible only with TM-polarized light, i.e., with a component of E normal to the surface. For all structures, near-field amplitude distributions (assuming an amplitude of the illuminating wave field equal to unity) and the SCS Q^{sc} as defined in Ref. 14 have been calculated. The scattering cross section is the energy radiated into the far field.

First, simulations were made for a circular cylinder with a radius of $r = 25\,\mathrm{nm}$. The structure is invariant in the third direction. Its SCS is shown in Fig. 1, and the near-field amplitude for the first two surface plasmons is shown in Fig. 2. A dipole excitation takes place at $\lambda = 250\,\mathrm{nm}$ and a quadrupole excitation at $\lambda = 214\,\mathrm{nm}$. The illumination direction is indicated by the arrows in Fig. 2. The near-field amplitude and the SCS are strongest for the quadrupole. The different resonances cannot be discriminated by looking only at the SCS.

To investigate the influence of the shape on the plasmon response, we analyzed elliptical cylinders. The radius of the minor axis is $r_1 = 10\,\mathrm{nm}$, and the radius of the major axis is $r_2 = 20\,\mathrm{nm}$. Figure 3 shows the SCS upon illumination from three directions (along the minor axis, along the major axis, and at an angle of 45°). It can be seen that two fundamental and relatively broad resonances appear at specific wavelengths for the two principal directions. Illumination along the minor axis excites the dipole at ≈266 nm, and illumination along the major axis excites a dipole at ≈181 nm. These fundamental plasmons are similarly excited after the structure is illuminated at an angle of 45° but with a somewhat lower

strength. It is obvious that the resonances are related to the principal axes of the structure and that illumination of the scatterer at an angle can be understood as a projection of the incoming wave on the main axes, resulting in excitation of both resonant plasmons. Additional higher-order plasmons are excited at appropriate wavelengths. The plasmons lead to a strongly enhanced amplitude in the near field and a huge SCS for only a small band of wavelength. The field distributions for the dipoles related to the principal axis and two supplementary excited quadrupoles are shown in Fig. 4. The quadrupoles are at $\lambda = 219\,\text{nm}$ for illumination of the particle under an angle of 45° and at $\lambda = 195\,\text{nm}$ for illumination along the major axis.

3. SCATTERING CROSS SECTION AND NEAR-FIELD AMPLITUDES FOR COUPLED PARTICLES

Coupled metallic nanoparticles are used, for example, in surface-enhanced Raman spectroscopy (SERS) experiments.[15] Recently they were used in single-molecule detection.[16] A specimen such as hemoglobin is placed between two metallic nanoparticles where field enhancement is highest. If the metallic particles are very close, the resulting field value between the two particles is enhanced in such a way that it may exceed the value from the single particle by orders of magnitude. This field enhancement makes it possible to excite a single molecule so strongly that its Raman spectrum can be detected.

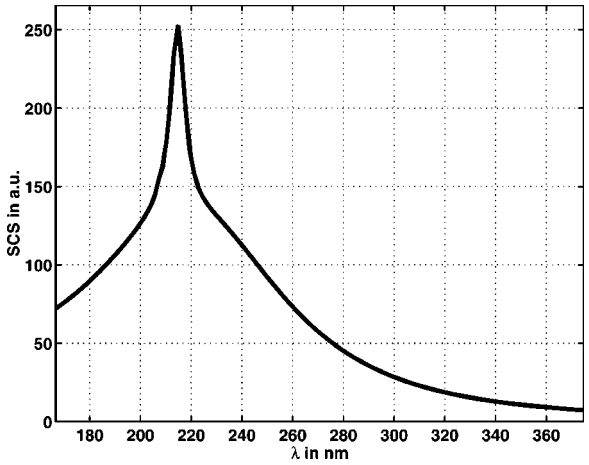

Fig. 1. SCS of a silver circular cylinder ($r = 25\,\text{nm}$), assuming a Drude model.

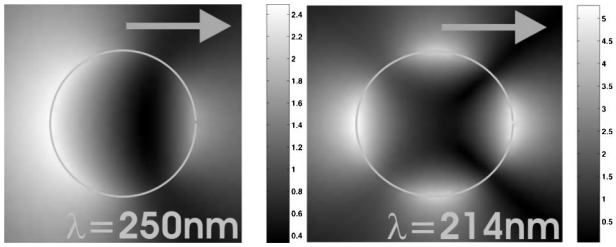

Fig. 2. Near-field amplitude for the excited plasmons (dipole and quadrupole).

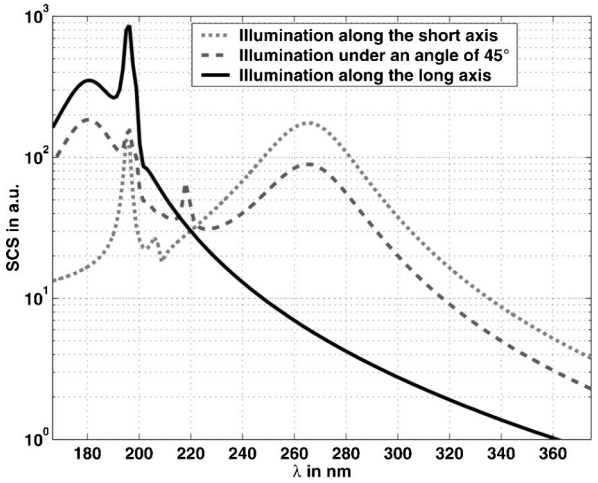

Fig. 3. SCS of a silver elliptical cylinder ($r_1 = 10\,\text{nm}$, $r_2 = 20\,\text{nm}$) assuming a Drude model.

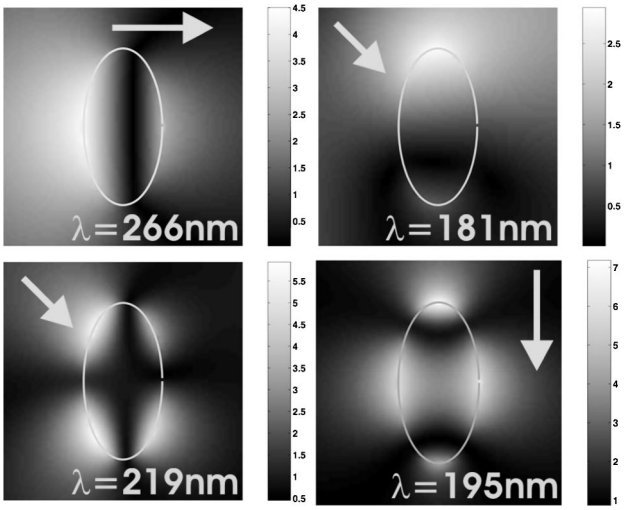

Fig. 4. Near field for various plasmons of a Drude–silver elliptical cylinder ($r_1 = 10\,\text{nm}$, $r_2 = 20\,\text{nm}$) at different wavelengths and illumination angles.

We have applied the BEM to the problem of the interaction of two coupled circular silver cylinders. They both have a radius of 25 nm. Again the Drude model for the permittivity was assumed. Figure 5 shows the SCS when the cylinders have a distance from surface to surface of 5 nm, under three different directions of illumination. In the present geometry an illumination angle of 0° means that the two cylinders are perpendicular to the illumination direction, and 90° means that they are in line with the illumination direction. It can be seen that the SCS shows a rather chaotic behavior for all three illumination directions, and a simple determination of the various plasmons is not possible anymore. Some of the generated field distributions of the surface plasmons can be seen in Fig. 6. The amplitudes after illumination of the two coupled nanocylinders at an angle of 90° (illumination is from above) are shown. In principle it can be said that the smaller the wavelength, the higher the nodal number of the excited surface plasmons. The fundamental mode appears at $\lambda = 303\,\text{nm}$. It is the most promising for SERS measurements, because a molecule situated

directly between the two resonant particles will be exposed to a homogenous field and a high field. We have to admit that this richness of plasmons will not be excited if the true refractive index of silver is assumed. Nonetheless, the fundamental mode will appear. For prediction of the behavior of the real system, the real values have to be taken into account (e.g., values published by Johnson and Christy[17]). Detailed theoretical investigations of coupled particles that take the experimental real refractive index values into account will be published elsewhere.

As the distance between the particles becomes larger, fewer plasmons are excited. The SCS becomes less turbulent and tends to the SCS of the single particle. As one can imagine, this is already the case for quite small distances if the illumination direction is perpendicular to the coupled particles, i.e., if the particles are not in the geometrical shadow. Figure 7 compares the SCS divided by two for the two particles under perpendicular illumination at a distance of 75 nm with the SCS of the single particle. They are qualitatively as well as quantitatively comparable. After calculating the field distributions around the particle, one can state that the same plasmons are excited as in the single-particle case. Therefore the particles can be treated as decoupled.

4. CONCLUSIONS

In this paper we have applied the boundary-element method (BEM) to the interaction of light with resonant metallic nanoparticles. We have presented a formulation for the BEM that makes it possible to treat coupled-particle systems. We have determined the SCS and corresponding near-field amplitude distributions of circular and elliptical cylinders. The elliptical structures have resonances in accordance with their geometrical axes, and illuminating the object at an angle to either axis will excite both resonances with an appropriately lower amplitude. We have treated the problem of coupled particles as they appear in SERS measurements. If the particles are close, various surface plasmons are excited. With increasing distance these turbulences will decrease, and from a certain distance that has been determined for two coupled circular silver cylinders perpendicular to the illumination direction, the system can be regarded as decoupled. SCS and amplitude near-field distributions then equal those of a single particle.

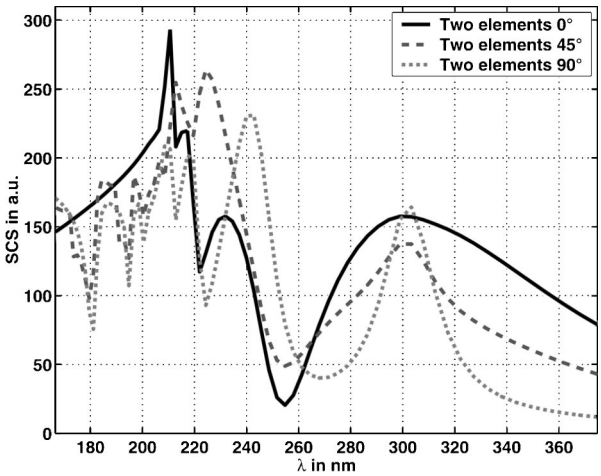

Fig. 5. SCS for two coupled silver circular cylinders ($r = 25$ nm) that have a surface separation of $d = 5$ nm, assuming a Drude model.

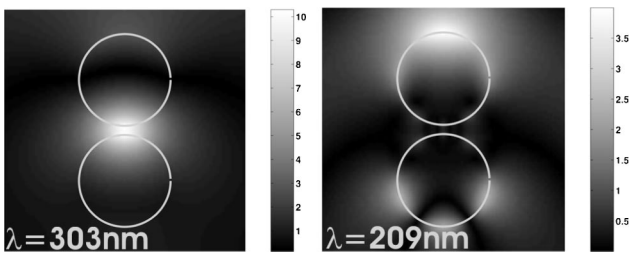

Fig. 6. Near-field amplitude after illumination of two coupled silver circular cylinders ($r = 25$ nm, $d = 5$ nm) from above at $\lambda_1 = 303$ nm and $\lambda_2 = 209$ nm.

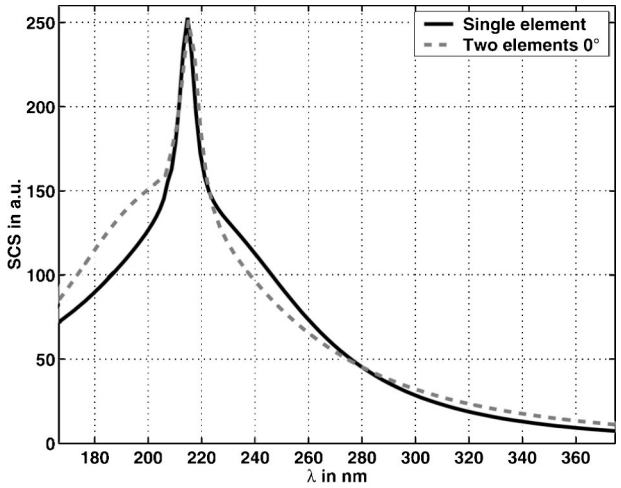

Fig. 7. SCS (divided by two) for two coupled silver circular cylinders ($r = 25$ nm, $d = 75$ nm) compared with that for a single cylinder.

ACKNOWLEDGMENT

The research was supported by the European Union within the framework of the Future and Emerging Technologies-SLAM program.

REFERENCES

1. M. Scharte, R. Porath, T. Ohms, M. Aeschlimann, J. R. Krenn, H. Ditlbacher, F. R. Aussenegg, and A. Liebisch, "Do Mie plasmons have a longer lifetime on resonance than off resonance?" Appl. Phys. B **73**, 305–310 (2001).
2. D. Wang, S. Guo, H. Ren, and S. Yin, "Optical characteristics of silver-doped polarizing glass," Opt. Lett. **27**, 992–994 (2002).
3. C. F. Bohren and D. R. Huffmann, *Absorption and Scattering of Light by Small Particles* (Wiley, New York, 1983).
4. E. Moreno, D. E. Erni, C. Hafner, and R. Vahldieck, "Multiple multipole method with automatic multipole setting applied to the simulation of surface plasmons in metallic nanostructures," J. Opt. Soc. Am. A **19**, 101–111 (2002).
5. W. H. Yang, G. C. Schatz, and R. P. Van Duyne, "Discrete dipole approximation for calculating extinction and Raman intensities for small particles with arbitary shape," J. Chem. Phys. **103**, 869–875 (1995).

6. J. P. Kottmann and O. J. F. Martin, "Accurate solution of the volume integral equation for high-permittivity scatterers," IEEE Trans. Antennas Propag. **48**, 1719–1726 (2000).
7. J. P. Kottmann and O. J. F. Martin, "Influence of the cross section and the permittivity on the plasmon-resonance spectrum of silver nanowires," Appl. Phys. B **73**, 299–304 (2001).
8. L. C. Wrobel and M. Aliabadi, *The Boundary Element Method* (Wiley, New York, 2002).
9. J. M. Bendickson, E. Glytsis, and T. K. Gaylord, "Focusing diffractive cylindrical mirrors: rigorous evaluation of various design methods," J. Opt. Soc. Am. A **18**, 1487–1494 (2001).
10. M. K. Choi, "Numerical calculation of light scattering from a layered sphere by the boundary-element method," J. Opt. Soc. Am. A **18**, 577–583 (2001).
11. J. Liu, B.-Y. Gu, B.-Z. Dong, and G.-Z. Yang, "Interference effect of dual diffractive cylindrical microlenses analyzed by rigorous electromagnetic theory," J. Opt. Soc. Am. A **18**, 526–536 (2001).
12. D. W. Prather, M. S. Mirotznik, and J. N. Mait, "Boundary integral method applied to the analysis of diffractive optical elements," J. Opt. Soc. Am. A **14**, 34–43 (1997).
13. D. W. Prather, J. N. Mait, M. S. Mirotznik, and J. P. Collins, "Vector-based synthesis of finite aperiodic subwavelength diffractive optical elements," J. Opt. Soc. Am. A **15**, 1599–1607 (1998).
14. M. Born and E. Wolf, *Principles of Optics* (Cambridge U. Press, Cambridge, UK, 1999).
15. M. Moskovits, "Surface-enhanced spectroscopy," Rev. Mod. Phys. **57**, 783–825 (1985).
16. H. Xu, E. J. Bjernfeld, M. Käll, and L. Börjesen, "Spectroscopy of single hemoglobin molecules by surface enhanced Raman scattering," Phys. Rev. Lett. **83**, 4357–4360 (1999).
17. P. B. Johnson and R. W. Christy, "Optical constants of the Nobel metals," Phys. Rev. B **6**, 4370–4379 (1972).